Correlation Pattern between Effective Radius and Optical Thickness of Water Clouds Simulated by a Spectral Bin Microphysics Cloud Model

Kentaroh Suzuki[1], Teruyuki Nakajima[1], Takashi Y. Nakajima[2], and Alexander Khain[3]
[1]*Center for Climate System Research, The University of Tokyo, Chiba, Japan*
[2]*Tokai University, Tokyo, Japan*
[3]*Institute of Earth Sciences, Hebrew University of Jerusalem, Jerusalem, Israel*

Abstract

The cloud particle size distribution of water clouds was simulated by a non-hydrostatic spectral bin microphysics cloud model. The result shows two different correlation patterns in the simulated optical thickness and effective radius; positive and negative correlations for non-drizzling and drizzling clouds, respectively, similar to the observed features reported by past remote sensing works.

The correlation pattern in a pristine condition is mainly composed by negative correlation with small fragment of positive correlation, similar to the satellite-observed characteristics over the FIRE region off California. In the case of polluted condition, on the contrary, only a positive correlation is simulated, similar to the satellite observation over the ASTEX region of North Atlantic Ocean. Satellite-observed contrast of correlation patterns between FIRE and ASTEX regions can be explained by the difference in the aerosol burden of airmasses over the two regions.

1. Introduction

Cloud feedback processes are recognized as a major source of uncertainty in understanding and predicting the climate change (Stephens 2005). The radiative effect of clouds plays a fundamental role in the climate system, and thus the cloud optical property is a key factor for determining the cloud radiative effect on climate. In this regard there have been many previous remote sensing studies of the cloud optical thickness and effective particle radius, which are main parameters to determine the cloud property, from aircraft (Nakajima and King 1990; Nakajima et al. 1991; Asano et al. 1995; Brenguier et al. 2000) and satellite image analysis (Han et al. 1994; Nakajima and Nakajima 1995; Kawamoto et al. 2001). These two parameters, by their definitions, are determined by the size distribution function of cloud particles and thus strongly depend on the cloud microphysical structure, which is recognized to depend on both aerosol amount and dynamical condition (e.g., Matsui et al. 2004). The combination of optical thickness and effective radius, therefore, contains useful information of the cloud particle growth process and provides a key link between cloud radiative property and microphysical characteristics of the cloud system.

The correlation pattern between cloud optical thickness and effective radius of low-level water clouds has been investigated by past several studies based on remote sensing results (Han et al. 1994, 1998; Asano et al. 1995; Boers and Rotstayn 2001; Nakajima and Nakajima 1995; Kawamoto et al. 2001; Szczodrak et al. 2001; Peng et al. 2002), since Nakajima et al. (1991) discovered that these optical parameters are positively correlated when the cloud is not drizzling and negatively correlated when the cloud includes a significant concentration of drizzle droplets. The positive correlation for non-drizzling cloud means that the cloud becomes optically thicker with particle growth, and the negative correlation for drizzling cloud indicates that the cloud becomes optically thinner with particle growth possibly due to loss of the cloud water by conversion to drizzle or rain water.

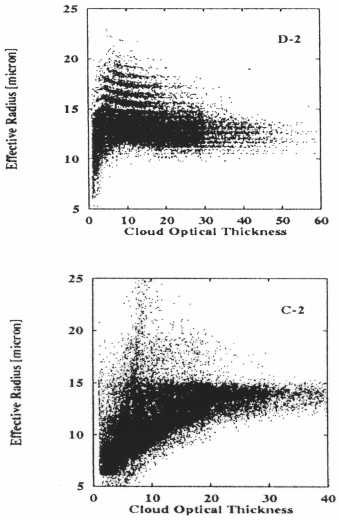

Fig. 1. Scatter plot between effective particle radius and optical thickness obtained from satellite observation over FIRE (upper) and ASTEX (lower) regions (cited from Nakajima and Nakajima 1995)

Nakajima and Nakajima (1995) investigated the correlation patterns over the FIRE (First ISCCP Regional Experiment) and ASTEX (Atlantic Stratocumulus Transition Experiment) regions, and found that the correlation pattern seems to be different between over these two regions. The typical examples of the scatter plot for FIRE and ASTEX regions are shown in Fig. 1, extracted from Figs. 17 and 18 of Nakajima and Nakajima (1995). The scatter plot over FIRE region is dominated by negative correlation with small part of positive correlation as shown in upper panel of Fig. 1, whereas the ASTEX region has only a positive correlation branch as shown in lower panel of Fig. 1. This implies that drizzle-rich clouds are more dominant over the FIRE region.

Modeling study will be useful for investigating the formation mechanisms of the two different correlation patterns. Recent progress in climate modeling of cloud microphysical process enables us to assess the global behavior of cloud microphysical property together with aerosol effect in terms of bulk parameterization (Menon et al. 2002; Lohmann and Lesins 2002; Suzuki et al. 2004). Lohmann et al. (2000) confirmed that the positive and negative correlations are obtained from non-precipitating and precipitating clouds, respectively, simulated by their General Circulation Model (GCM). In order to interpret the observed correlation pattern from a cloud microphysical point of view, however, it is necessary to perform a numerical simulation by cloud models with more detailed representation of microphysical processes than that of GCMs that are based on simplified parameterization of cloud microphysics. Such detailed microphysical cloud models

Corresponding author: Teruyuki Nakajima, Center for Climate System Research, The University of Tokyo, 5-1-5 Kashiwanoha, Kashiwa, Chiba 277-8568, Japan. E-mail: teruyuki@ccsr.u-tokyo.ac.jp.

have been recently developed and used for numerical experiments (e.g., Feingold et al. 1999; Feingold and Kreidenweis 2002; Khain and Sednev 1996; Khain et al. 2004; Takahashi and Kawano 1998; Takahashi and Shimura 2004).

In this paper we briefly report the result of the statistics of optical thickness and effective radius of water clouds simulated by a non-hydrostatic spectral microphysics cloud model to provide an interpretation for satellite-observed correlation patterns. Because the model used in this simulation explicitly predicts the size distribution function of cloud particles, the simulated result provides us with more detailed insight into the mechanisms underlying the correlation pattern than previous studies based on observations and GCM simulation.

2. Model simulation

In order to investigate the cloud microphysical processes in detail we adopted the non-hydrostatic spectral bin microphysics cloud model, which has been reconstructed from the original model of Khain and Sednev (1996) and Khain et al. (2004). In this model the size distribution function of liquid cloud particles is explicitly predicted taking into account the various microphysical processes, i.e., nucleation from aerosol, condensational growth, and collision-coagulation process.

The nucleation process is calculated from the size distribution function of hygroscopic aerosols, which is also predicted in the model. We prepared 20 bins ranging from 0.01 μm to 1 μm for aerosol size spectra and 60 bins from 3 μm to 3000 μm for cloud particle size spectra. The part of aerosol population greater than the critical size is activated to grow into cloud particles. This critical radius of aerosol is calculated from the supersaturation according to the Kohler theory. The sulfate aerosol (ammonium sulfate) was assumed for chemical species in the simulation. The number concentration of aerosols beyond the critical size is added to the minimum size bin of cloud particle (3 μm). The number of aerosols belonging to size bins greater than the critical size becomes zero after the nucleation.

The nucleated cloud particle grows by condensation and collision-coagulation processes in the model. The prognostic equation for cloud size spectra $f(m, t)$ by these processes is given as (e.g., Rogers and Yau 1989)

$$\frac{\partial}{\partial t}f(m,t) = -\frac{\partial}{\partial m}\left(f(m,t)\frac{dm}{dt}\right) + \frac{1}{2}\int_0^m f(m',t)f(m-m',t)K(m',m-m')\,dm' - f(m,t)\int_0^{+\infty} f(m',t)K(m,m')\,dm',$$

where m denotes the mass of a cloud particle and t denotes the time. The first term on the right hand side represents the condensation process, and the second and third terms represent the collision-coagulation process. The growth speed of condensation is determined by supersaturation S as

$$\frac{dm}{dt} = rG(p,T)S, \tag{1}$$

where r denotes the particle radius and $G(p, T)$ is a function of pressure p and temperature T given as

$$G(p,T) = 4\pi\left[\left(\frac{L}{R_vT}-1\right)\frac{L}{KT}+\frac{R_vT}{De^*(T)}\right]^{-1},$$

where L, R_v, K, D, and $e^*(T)$ are the latent heat, gas constant for water vapor, thermal conductivity, diffusion coefficient for water vapor and saturation vapor pressure at temperature T, respectively. The growth speed is positive (condensation) when the supersaturation S is positive and negative (evaporation) when the supersaturation S is negative. The supersaturation S is determined from the balance between condensation or evaporation and cooling of air by upward motion. The collection kernel function $K(m_1, m_2)$ for the collision-coagulation process is assumed to have the form suggested by Long (1974), according to which the collision-coagulation process is active only when the size of larger particles exceeds 50 μm. In the present model we adopt the numerical schemes of Bott (1989) for calculating the condensation process and Bott (1998) for collision-coagulation process because of their numerical stability, conservative property, and positive definiteness. The gravitational settling process for liquid water particles is also incorporated into the model by assuming the terminal fall velocity as a function of particle size.

We perform a two-dimensional numerical experiment to generate a low-level water cloud by giving a horizontally homogeneous initial condition as shown in Fig. 2. The stable layer above around 1km and convectively unstable layer in lower atmosphere are assumed as shown in Fig. 2(a) and (b). The vertical shear of horizontal wind is also given in the initial condition as shown in Fig. 2(c). We initially assume the Junge-type size distribution function for aerosol particle as

$$f_{aero}(z,r) = f_0(z)\left(\frac{r}{r_0}\right)^{-3},$$

where $r_0 = 0.1$ μm and $f_0(z)$ is the value of f_{aero} at $r=r_0$, which is given as an exponential decay profile as

$$f_0(z) = f_{sfc}\exp\left(-\frac{z}{H}\right), \tag{2}$$

where f_{sfc} and H denote the value of f_0 at ground level and the scale height, respectively. We changed the aerosol burden by changing the values of f_{sfc} from $f_{sfc}=10^5$ m^{-3} to 10^7 m^{-3} for investigating the aerosol effect on the cloud property, and the scale height H was set to 1 km. Values of $f_{sfc}=10^5$ m^{-3} and 10^7 m^{-3} approximately correspond to aerosol particle number concentrations of $n_a=10^8$ m^{-3} and 10^{10} m^{-3}, respectively, and also to column aerosol particle numbers of $N_a=10^{11}$ m^{-2} and 10^{13} m^{-2}, respectively, with the 1 km scale height. A warm-bubble is initially located to trigger convection and cloud formation as a potential temperature perturbation $\Delta\theta$ following Gallus and Rancic (1996) as

$$\Delta\theta = \Delta\theta_0\cos^2\left(\frac{\pi}{2}\sqrt{\left(\frac{x-x_0}{x_r}\right)^2+\left(\frac{z-z_0}{z_r}\right)^2}\right),$$

where $x_0=9$ km, $z_0=0.5$ km, $x_r=5$ km, $z_r=0.5$ km, and $\Delta\theta_0=1$K. The computational domain is set as 30 km in horizontal and 5 km in vertical, and the resolutions are 500 m in horizontal and 50 m in vertical.

We divide the cloud size distribution ranging from 3 μm to 3000 μm into three parts, i.e., 3–30 μm, 30–300 μm, and 300–3000 μm, and represent each range as cloud, drizzle, and rain water part, respectively. The mass concentrations of cloud, drizzle, and rain can be calculated by integrating the simulated size distribution over these ranges. As an advantage of spectral bin microphysics model, we can explicitly calculate the optical thickness and effective radius from the simulated size distribution function $f(x, z, r)$ for each grid point (x, z) by their definitions as

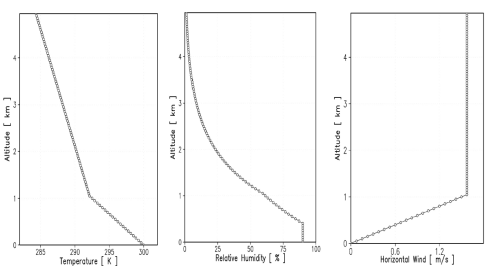

Fig. 2. Initial profiles assumed for the present numerical simulation (a: temperature, b: relative humidity, c: horizontal wind).

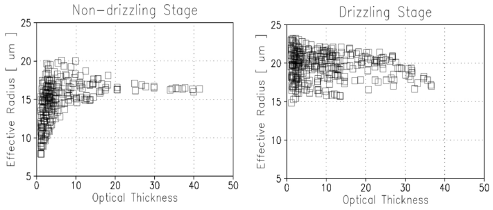

Fig. 3. Scatter plots between effective radius and optical thickness obtained from the simulation for the clouds at non-drizzling stage (left) and drizzling stage (right).

$$\tau_c(x) = \int_{z=z_B}^{z=z_T} \int_{r=3\,\mu m}^{r=30\,\mu m} Q_{ext} f(x,z,r)\,\pi r^2 dr dz,$$

$$r_e(x,z) = \frac{\int_{r=3\,\mu m}^{r=30\,\mu m} f(x,z,r)\,r^3 dr}{\int_{r=3\,\mu m}^{r=30\,\mu m} f(x,z,r)\,r^2 dr}$$

where Q_{ext} is the extinction coefficient factor and equals to 2 in good approximation for cloud particles, and z_B and z_T denote the cloud base and cloud top, respectively. Because satellite-measured r_e reflects an in-cloud value at 20–40% of the total optical thickness from the cloud top (Nakajima and King 1990), we adopt the value of r_e computed at 30% of the total optical thickness so that it is comparable with satellite retrievals.

3. Result and discussion

Figure 3 shows a scatter plot of effective radius and optical thickness obtained from the composite of simulated results with f_{sfc} assumed in equation (2) ranging from f_{sfc}= 10^5 m^{-3} to f_{sfc}=10^6 m^{-3}, approximately corresponding to aerosol particle number concentration of n_a=10^8 m^{-3} and 10^9 m^{-3}, respectively. Each point in Fig. 3 represents the cloud state at a particular time and a particular spatial grid. We divided the cloud state into two groups, i.e., non-drizzling stage as shown in the left panel and drizzling stage as shown in the right panel of the figure. The plot is separated into the two groups according to time. In particular, the cloud states before the time at which the maximum drizzle water content becomes greater than 10^{-3} gm^{-3} are assigned to 'non-drizzling stage' and the cloud states after that time are classified as 'drizzling stage' for each simulation. It is clearly illustrated in Fig. 3 that the effective radius and optical thickness are positively correlated when the cloud is at the stage before drizzling (left panel) for small optical thickness and negatively correlated when the cloud is at the drizzling stage (right panel). These features are similar to those obtained by previous observational works by Nakajima et al. (1991) and Han et al. (1994), and also by GCM work by Lohmann et al. (2000).

The positive and negative correlations found in the simulated r_e- τ_c scatter plot can roughly be understood from a microphysical point of view as explained below. It is useful to consider a simplified conceptual model for a uniform cloud with a single particle size, where the column cloud particle number is N_c, liquid water path is W, particle radius is r, and the optical thickness is τ. Combination of W=$N\rho_w 4/3\pi r^3$ and τ=$2\pi N r^2$ leads to the relationships $r \sim W^{1/3}N^{-1/3}$ and $\tau \sim W^{2/3}N^{1/3}$. For the clouds at the non-drizzling stage dominated by condensational growth process, N tends to be constant and W increases, leading to the increase in both r and τ, and thus positive correlation between them. For the clouds at the drizzling stage, on the contrary, collision-coagulation process is active instead of condensational growth to stop increasing W, and N starts to decrease, resulting the decrease in τ with increasing r to cause a negative correlation between them. Note that the slope of negative correlation shown in right panel of Fig. 3 is stronger than $r_e \sim \tau_c^{-1}$, indicating that W decreases with particle growth due to the loss of cloud water by conversion into drizzle or rain water. This feature is also consistent with previous remote sensing studies by Nakajima et al. (1991) and Nakajima and Nakajima (1995).

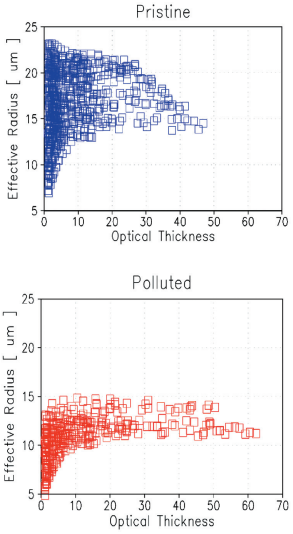

Fig. 4. Scatter plots between effective particle radius and optical thickness obtained from the simulation for pristine (upper) and polluted (lower) air conditions.

A sensitivity experiment to change the aerosol concentration assumed in the initial condition is also performed to investigate the aerosol effect on the $r_e - \tau_c$ correlation pattern. The value of f_{sfc}, assumed in equation (2), is changed from f_{sfc}=10^5 m^{-3} to f_{sfc}= 10^7 m^{-3}. These values of f_{sfc} approximately correspond to the surface aerosol number concentrations of n_a=10^8 m^{-3} and 10^{10} m^{-3}, respectively. Simulated results for the condition of surface aerosol number concentration n_a smaller than 10^9 m^{-3} (assigned as 'pristine condition') are shown in the upper panel of Fig. 4 and the results for n_a greater than 10^9 m^{-3} (assigned as 'polluted condition') are shown in the lower panel of Fig. 4. There is a distinctive difference between the simulated scatter plots for pristine and polluted conditions. The scatter plot for pristine condition (Fig. 4 upper panel) has a large portion of negative correlation with only a small part of positive correlation, whereas the scatter plot for polluted condition (Fig. 4 lower panel) has only a positive correlation branch. The former and latter feature closely resembles the satellite-observed characteristics over FIRE and ASTEX regions, respectively, reported by Nakajima and Nakajima (1995), shown in upper and lower panel of Fig. 1.

The simulated scatter plot for pristine condition shown in the upper panel of Fig. 4 is characterized by a large portion of negative correlation with lack of positive correlation part except for a small segment. These characteristics are very similar to those observed over the FIRE region off California by Nakajima and Nakajima (1995) shown in upper panel of Fig. 1. In this case the cloud becomes optically thicker with particle growth indicated by the small part of positive correlation at the early stage before drizzling, followed by active formation of drizzle particles illustrated by the large portion of negative correlation.

In the polluted case shown in the lower panel of Fig. 4, on the contrary, only a positive correlation is found, indicating that non-drizzling clouds are dominant in this case. Under the polluted condition, abundant aerosol particles produce numerous cloud particles and the supersaturation is limited to lower values due to large consumption of water vapor by condensation of numerous cloud particles. The low value of supersaturation delays the condensational growth as given by equation (1), and thus the cloud particle cannot reach a size large enough to activate the collision-coagulation process. This is the reason why we have only the positive correlation branch for polluted condition. This positively

correlated feature is very similar to the observed characteristics over ASTEX region of North Atlantic Ocean by Nakajima and Nakajima (1995) shown in lower panel of Fig. 1.

It is concluded from the above discussion that the correlation pattern between optical thickness and effective radius is significantly affected by aerosol amount, and the simulated correlation patterns for pristine and polluted air condition have closely similar features to satellite observation over FIRE and ASTEX regions, respectively. This result suggests that the satellite-observed difference in r_e–τ_c correlation pattern between FIRE and ASTEX regions can be explained by a difference in the aerosol amount over these regions. In fact it is known from satellite observation of aerosols (e.g., Husar et al. 1997; Higurashi and Nakajima 1999) that the aerosol amount over FIRE and ASTEX region is distinctively different, that is, the FIRE region is comparatively pristine and the ASTEX region is polluted. Such difference in the aerosol burden causes the different growth patterns of cloud particles as depicted by the contrast of r_e–τ_c correlation patterns in our model simulation.

4. Conclusion

In this study we performed the numerical simulation of water cloud optical properties with a spectral bin microphysics cloud model, and investigated the correlation pattern between effective radius and optical thickness. It is found that the model calculation well simulated the observed r_e–τ_c correlation pattern. These parameters are positively and negatively correlated in case of non-drizzling and drizzling clouds, respectively, in agreement with previous observational studies.

It was revealed that the simulated r_e–τ_c correlation pattern is significantly affected by aerosol amount. The correlation pattern for pristine condition resembles the satellite-observed one over FIRE region off California, in which the negative correlation is dominant, accompanied by a small portion of positive correlation. The simulated correlation for polluted condition, on the contrary, reproduced the similar feature to satellite observation over ASTEX region of North Atlantic Ocean, dominated by positive correlation. It is suggested that the observed difference in the r_e–τ_c correlation pattern can be interpreted as the manifestation of difference in cloud microstructure induced by the different aerosol amount over these regions.

Acknowledgement

This research was supported by Global Environment Research Fund by Ministry of Environment Japan B–4; RR2002 project of Ministry of Science, Sports, and Culture; JAXA/ADEOS-II GLI project.

References

Asano, S., M. Shiobara, and A. Uchiyama, 1995: Estimation of cloud physical parameters from airborne solar spectral reflectance measurements for stratocumulus clouds, *J. Atmos. Sci*., **52**, 3556–3576.

Boers, R., and L. D. Rotstayn, 2001: Possible links between cloud optical depth and effective radius in remote sensing observations, *Quart. J. Roy. Meteor. Soc*., **127**, 2367–2383.

Bott, A., 1989: A positive definite advection scheme obtained by nonlinear renormalization of the advective fluxes, *Mon. Wea. Rev*., **117**, 1006–1015.

Bott, A., 1998: A flux method for the numerical solution of the stochastic collection equation, *J. Atmos. Sci*., **55**, 2284–2293.

Brenguier, J.-L., H. Pawlowska, L. Schuller, R. Preusker, J. Fischer, and Y. Fouquart, 2000: Radiative properties of boundary layer clouds: Droplet effective radius versus number concentration, *J. Atmos. Sci*., **57**, 803–821.

Feingold, G., W. R. Cotton, S. M. Kreidenweis, and J. T. Davis, 1999: The impact of giant cloud condensation nuclei on drizzle formation in stratocumulus: Implications for cloud radiative properties, *J. Atmos. Sci*., **56**, 4100–4117.

Feingold, G., and S. M. Kreidenweis, 2002: Cloud processing of aerosol as modeled by a large eddy simulation with coupled microphysics and aqueous chemistry, *J. Geophys. Res*., **107(D23)**, 4687, doi:10.1029/2002JD002054.

Gallus, W. A., and M. Rancic, 1996: A non-hydrostatic version of the NMC's regional Eta model, *Quart. J. Roy. Meteor. Soc*., **122**, 495–513.

Han, Q., W. B. Rossow, and A. A. Lacis, 1994: Near-global survey of effective droplet radii in liquid water clouds using ISCCP data, *J. Climate*, **7**, 465–497.

Han, Q., W. B. Rossow, J. Chou, and R. M. Welch, 1998: Global survey of the relationships of cloud albedo and liquid water path with droplet size using ISCCP, *J. Climate*, **11**, 1516–1528.

Higurashi, A., and T. Nakajima, 1999: Development of a two-channel aerosol retrieval algorithm on a global scale using NOAA AVHRR, *J. Atmos. Sci*., **56**, 924–941.

Husar, R. B., J. M. Prospero, and L. L. Stowe, 1997: Characterization of tropospheric aerosols over the oceans with the NOAA advanced very high resolution radiometer optical thickness operational product, *J. Geophys. Res*., **102(D14)**, 16889–16909.

Kawamoto, K., T. Nakajima, and T. Y. Nakajima, 2001: A global determination of cloud microphysics with AVHRR remote sensing, *J. Climate*, **14**, 2054–2068.

Khain, A., A. Pokrovsky, A. Pinsky, A. Seifeld, and V. Phillips, 2004: Simulation of effects of atmospheric aerosols on deep turbulent convective clouds using a spectral microphysics mixes-phase cumulus cloud model. Part I: Model description and possible applications. *J. Atmos. Sci*., **61**, 2963–2982.

Khain, A., and I. Sednev, 1996: Simulation of precipitation formation in the Eastern Mediterranean coastal zone using a spectral microphysics cloud ensemble model. *Atmos. Res*., **43**, 77–110.

Lohmann, U., G. Tselioudis, and C. Tyler, 2000: Why is the cloud albedo-particle size relationship different in optically thick and optically thin clouds? *Geophys. Res. Lett*., **27**, 1099–1102.

Lohmann, U., and G. Lesins, 2002: Stronger constraints on the anthropogenic indirect aerosol effect, *Science*, **298**, 1012–1015.

Long, A. B., 1974: Solutions to the droplet collection equation for polynomial kernels, *J. Atmos. Sci*., **31**, 1040–1052.

Matsui, T., H. Masunaga, R. A. Pielke Sr., and W.-K. Tao, 2004: Impact of aerosols and atmospheric thermodynamics on cloud properties within the climate system, *Geophys. Res. Lett*., **31**, L06109, doi:10.1029/2003GL019287.

Menon, S., A. D. del Genio, D. Koch, and G. Tselioudis, 2002: GCM simulations of the aerosol indirect effect: Sensitivity to cloud parameterization and aerosol burden, *J. Atmos. Sci*., **59**, 692–713.

Nakajima, T., and M. D. King, 1990: Determination of the optical thickness and effective particle radius of clouds from reflected solar radiation measurements. Part I: Theory. *J. Atmos. Sci*., **47**, 1878–1893.

Nakajima, T., M. D. King, and J. D. Spinhirne, 1991: Determination of the optical thickness and effective particle radius of clouds from reflected solar radiation measurements. Part II: Marine stratocumulus observations. *J. Atmos. Sci*., **48**, 728–750.

Nakajima, T. Y., and T. Nakajima, 1995: Wide-area determination of cloud microphysical properties from NOAA AVHRR measurements for FIRE and ASTEX regions. *J. Atmos. Sci*., **52**, 4043–4059.

Peng, Y., U. Lohmann, R. Leaitch, C. Banic, and M. Couture, 2002: The cloud albedo-cloud droplet effective radius relationship for clean and polluted clouds from RACE and FIRE.ACE. *J. Geophys. Res*., **107(D11)**, 4106, doi:10.1029/2000JD000281.

Rogers, R. R., and M. K. Yau, 1989: *A short course in cloud physics*. 3rd edition, Pergamon Press, 293 pp.

Stephens, G. L., 2005: Cloud feedbacks in the climate system: A critical review, *J. Climate*, **18**, 237–273.

Suzuki, K., T. Nakajima, A. Numaguti, T. Takemura, K. Kawamoto, and A. Higurashi, 2004: A study of the aerosol effect on a cloud field with simultaneous use of GCM modeling and satellite observation, *J. Atmos. Sci*., **61**, 179–194.

Szczodrak, M., P. H. Austin, and P. B. Krummel, 2001: Variability of optical depth and effective radius in marine stratocumulus clouds, *J. Atmos. Sci*., **58**, 2912–2926.

Takahashi, T., and T. Kawano, 1998: Numerical sensitivity study of rainband precipitation and evolution, *J. Atmos. Sci*., **55**, 57–87.

Takahashi, T., and K. Shimura, 2004: Tropical rain characteristics and microphysics in a three-dimensional cloud model, *J. Atmos. Sci.*, **61**, 2817–2845.

Manuscript received 15 May 2006, accepted 4 July 2006
SOLA: http://www.jstage.jst.go.jp/browse/sola/